International Space Station Leak Localization Using Attitude Response Data

Jong-Woo Kim,[*]

John L. Crassidis,[†]

Srinivas R. Vadali,[‡]

Adam L. Dershowitz[§]

Abstract

This paper presents a new method to localize air leaks on the International Space Station based on the spacecraft attitude and rate behavior produced by a mass expulsion force of the leaking air. Thrust arising from the leak generates a disturbance torque, which is estimated using a real-time Unscented filter with a dynamical model, including external disturbances such as aerodynamic drag and gravity-gradient. The leak location can be found by estimating the moment arm of the estimated disturbance torque, assuming that leak is caused by only one hole. Knowledge of the vent thrust magnitude and its resulting disturbance torque are needed to estimate the moment arm. The vent thrust direction is assumed to be perpendicular to the structure surface and its magnitude is determined using a extended Kalman filter with a nozzle dynamics model. There may be multiple leak locations for a given response, but the actual geometric structure of the space station eliminates many of the possible solutions. Numerical results show that the leak localization method is very

[*]Graduate Student, Department of Aerospace Engineering, Texas A&M University, College Station, TX 77843-3141. Currently Senior Engineer, Mechatronics and Manufacturing Technology Center Corporate Technology Operations, Samsung Electronics CO., LTD., 416 Maetan-3 Dong, Yeongtong-Gu, Suwon-City, Gyeonggi-Do, Korea 443-742. Member AIAA.

[†]Associate Professor, Department of Mechanical and Aerospace Engineering, University at Buffalo, The State University of New York, Amherst, NY 14260-4400. Associate Fellow AIAA.

[‡]Professor, Department of Aerospace Engineering, Texas A&M University, College Station, TX 77843-3141. Associate Fellow AIAA.

[§]Senior Engineer, Exponent, Failure Analysis Associates, 5401 McConnell Avenue Los Angeles, CA 90066. Member AIAA.

efficient when used with the conventional sequential hatch closure or airflow induction sensor system.

Introduction

The International Space Station (ISS) is orbiting in a 51.6° inclination near-circular low-Earth-orbit (LEO) with an altitude between 370 and 460 km, and is expected to have a minimum operational lifetime of 15 years. Because of the large structure, long lifetime and orbit characteristics,[1] the ISS may be subject to impacts from hypervelocity particles such as micro-meteorites and space debris that can severely damage the station. This damage may threaten the safety of the crew if the pressurized wall of a module is perforated, which may result in significant air loss. Collisions with other objects are another possible cause of a leak, as occurred on the Russian Space Station Mir in 1997. To protect the ISS from the impact damages, various debris shields have been designed. Heavy shields are placed in the forward facing area which is likely to be hit frequently, and fewer shields are used in the nadir-facing and aft area.[2] Hazards associated with a debris penetration of the ISS modules are discussed in Ref. 3.

Perforations in a pressurized module will result in a rapid temperature and pressure decrease. Therefore, fast determination of the extent and location of the leak is needed to maintain the operational status in order to provide safety for the crew. The first indication of a leak in the ISS is the depressurization of a module. The leak size can be calculated by measuring the internal pressure and its depressurization rate. Based on the extent of leak it is possible to calculate the "reserve time" left until a crew evacuation is required. Depending on the reserve time operational decisions must be made, including: 1) whether or not to perform a leak isolation to patch the leak, or 2) evacuate the ISS. Leak localization should be performed first to find the leaking module. Then, the exact location within the leaking module can be determined for repair purposes. The effects of a compartment vent flow during the spacecraft launch has been surveyed in Ref. 4. Also in Ref. 5, a closed form equation has been derived to calculate the pressure differentials across the walls of

compartment as a function of external and internal pressure changes.

Conventional methods to locate air leaks on the ISS include the sequential module leak isolation process for the US segment (prior to assembly stage 10A) and the airflow induction sensor system for the Russian segment. The sequential module leak isolation process involves having the crew close hatches sequentially while monitoring the pressure difference across each hatch. A drawback of this process is that a very small pressure difference can keep a closed hatch from being open again, which significantly reduces the reserve time and can pose an immediate risk to the crew. Thus, safety dictates that the hatches be closed in an order that will never trap a crew member away from the escape vehicle. This may significantly inhibit the leak isolation process if the leaking module is not located within the first few hatch closures.

The airflow induction sensor system employs hot-wire anenometers situated in hatchways to measure the air flow direction and its rate. The hot-wire anenometer operates by air passing across a wire with a current running through it to maintain a constant temperature in the wire. These devices are installed at all hatchways of the Russian segment. However, the airflow induction sensor system designed for the ISS has several limitations for the following reasons. The sensors are not mounted at all hatchways of the US segment (only at Node-2 and Node-3 of the US segment). Therefore, the sequential module isolation process is still needed to determine which module leaks in the US segment. Since the sensors are very sensitive to the air circulation inside, the venting system and the movement of the crew must be stopped for several minutes, which may waste time in an emergency situation. Because these sensors are situated in hatchways, the location of the leak within the suspected leaking module cannot be found for repair purposes without using other inspection processes (this is also true for the sequential isolation process). Therefore, a more efficient localization system is needed to locate the leaks.

The new method presented in this paper uses the attitude response of the ISS caused by the leak reaction force of the air flowing through a perforated hole. The vent thrust can

yield a strong reaction torque depending on the size and location of the leak. A leak hole on the surface of a pressurized module can be modeled as a short nozzle with the leaking air as the propellant. We assume that the line of action of the vent thrust is perpendicular to the cross section area of the leak hole. This assumption is reasonable due to the relatively thin skin of each module. The effects of the reaction torque due to a vent thrust can be found in Ref. 4.

Based on the nozzle dynamics, an extended Kalman filter (EKF) algorithm is used to estimate the vent thrust magnitude with the internal pressure measurements. The venting torque is estimated by the Unscented filter (UF) developed by Julier and Uhlman.[6] The vent torque, which is not explicitly modeled in the attitude dynamics, shows up as a residual disturbance torque when the spacecraft angular rate measurement undergoes a filtering process. In the disturbance torque estimation algorithm, the filter state vector is augmented to include the unknown parameters as additional states, resulting in a total of six states, where three states are for the total angular momentum of the spacecraft and the remaining three states are for the three-axis components of the disturbance torque. But problems arise when the unmodeled disturbances, besides the vent torque, dominate the residual torque.

Among the external disturbances, the aerodynamic torque is known to have large uncertainties in its parameters, but has relatively less effect on the residual disturbance torque estimation results compared to the uncertainties in the inertia components of the ISS in a short period. Therefore, parameter estimation methods are employed to estimate the six inertia components when it is known that a venting leak does not occur on the spacecraft. The UF algorithm is employed to estimate the inertia in real time. It is shown that the complete inertia parameters are unobservable when the space station attitude is in its torque equilibrium attitude (TEA), which is the nominal ISS operational attitude. But the inertia observability can be strengthened with the presence of attitude maneuvers. Problems in estimating the inertia matrix for the ISS have been investigated in several papers, such as Refs. 7 and 8. In Ref. 9, small sinusoidal probing signals are used to enhance the observability of the

inertia by causing attitude motion about the TEA. Also in Ref. 8, an estimation algorithm to determine the mass and aerodynamic torque properties of the ISS in LEO, based on a least-squares method, has been derived with the use of an indirect adaptive control algorithm to enhance the observability of the unknown parameters.

The possible locations of the air leak are then calculated using the estimated vent torque, vent thrust magnitude and the actual geometric structure of the pressurized segments. For simplicity, the disturbance torque caused by the pressure of the impingement of the leaking air plume on nearby surfaces is neglected. The effects of plume impingement are found in Refs. 10 and 11. Also, we assume that the leak is caused by a single leak hole. There may be single or multiple leak locations that produce the same attitude response. To reduce the number of possible solutions, conventional methods are combined with the new leak localization method. This approach reduces the number of possible solutions, so that fewer hatch closures are required to uniquely determine the leak location. Advantages of the attitude response method include: 1) No other devices are needed besides pressure gauges to measure the air pressure, and spacecraft attitude and rate sensors; 2) Relatively fast leak localization can be achieved compared to the conventional leak localization method proposed for the ISS; and 3) The new method not only determines the possible leaking modules but also determines the possible locations of the leak hole within those modules. This may be critical to allow for repairs rather than sealing off a module or performing a station evacuation.

The remainder of this paper is organized as follows. First, a summary of the attitude dynamics for the ISS is given. Then, using isentropic nozzle theory, the vent thrust is calculated using isentropic and isothermal air depressurization models. Next, a derivation of the disturbance torque estimation process is given. Then, the steps to locate a leak are described using the calculated disturbance torque and the thrust due to a leak. Finally, numerical simulations for the leak localization are presented with conclusions.

Spacecraft Attitude Dynamics

The rotational dynamic equations of motion for a rigid spacecraft in a LEO environment, expressed in a body-fixed frame, are given by Euler's equation:

$$\dot{\boldsymbol{H}}(t) = -\left\{ J^{-1}\left[\boldsymbol{H}(t) - \boldsymbol{h}(t)\right] \right\} \times \boldsymbol{H}(t) + \boldsymbol{N}_{drag}(t) + \boldsymbol{N}_{grav}(t) + \boldsymbol{N}_{vent}(t) \qquad (1)$$

where $\boldsymbol{H}(t)$ is the total angular momentum of the spacecraft satisfying

$$\boldsymbol{H}(t) = J\boldsymbol{\omega}(t) + \boldsymbol{h}(t) \qquad (2)$$

and J is the inertia matrix about the center of mass, $\boldsymbol{\omega}(t)$ is the angular velocity of the spacecraft with respect to an inertial frame, $\boldsymbol{N}_{drag}(t)$ is the aerodynamic torque, $\boldsymbol{N}_{grav}(t)$ is the gravity-gradient torque, $\boldsymbol{h}(t)$ is the angular momentum of the control moment gyroscopes (CMGs), and $\boldsymbol{N}_{vent}(t)$ is the torque due to an air leak vent. Other environmental effects such as solar radiation and Earth's albedo are neglected for simplicity and lack of data for the space station's optical properties. But the solar radiation torque can still be significant during periods of low solar activity (for more details refer to Refs. 12 and 13). The rotational dynamical effects caused by solar arrays rotations are omitted because of their slow motion (1Hz/orbit) and their relatively small inertia (3.4%) and mass (1.5%) compared to the total ISS inertia and its mass at assembly stage UF1.[1] However, the drag model does contain the effects of the solar arrays on the resulting aerodynamic torques because of their large surface area.

The gravity-gradient torque for an orbiting spacecraft, neglecting the $J2$ effect, is[13]

$$\boldsymbol{N}_{grav}(t) = \frac{3\mu}{||\boldsymbol{R}_S(t)||^3} \int \left[\boldsymbol{r}_i \times \hat{\boldsymbol{R}}_S(t)\right] \left[\boldsymbol{r}_i \cdot \hat{\boldsymbol{R}}_S(t)\right] dm_i = \frac{3\mu}{||\boldsymbol{R}_S(t)||^3} \hat{\boldsymbol{R}}_S(t) \times \left[J\hat{\boldsymbol{R}}_S(t)\right] \quad (3)$$

where $\mu \simeq 3.986 \times 10^{14}$ m^3/s^2 is the Earth gravitational constant and $\hat{\boldsymbol{R}}_S(t)$ is the unit vector from the Earth center to the spacecraft body frame's origin. The mass element of the

spacecraft is dm_i and its position with respect to the center of mass is $\boldsymbol{r}_i$. Equation (3) can be rewritten as

$$\boldsymbol{N}_{grav}(t) = 3n^2 \boldsymbol{C}_3(t) \times J\,\boldsymbol{C}_3(t) \tag{4}$$

where $\boldsymbol{C}_3(t) = -\hat{\boldsymbol{R}}_S(t)$ is the 3rd column of the direction cosine matrix, C, from the local-vertical-local-horizontal (LVLH) orbital reference frame to the body-fixed reference frame. The orbital frequency $n = \sqrt{\mu/\|\boldsymbol{R}_S(t)\|^3}$ can be calculated from the orbit data of the spacecraft (for the ISS, $n \simeq 0.0011\,\text{rad/s}$).

The aerodynamic torque, $\boldsymbol{N}_{drag}(t)$, is modeled such that the drag force and the center of pressure location are functions of the attitude of the spacecraft:

$$\boldsymbol{N}_{drag}(t) = -\frac{1}{2}\rho_a(t)|\mathbf{v}_r(t)|C_D\,S(t)\left[\boldsymbol{\rho}_{cp}(t) \times \mathbf{v}_r(t)\right] \tag{5}$$

where $v_r(t)$ is the relative velocity vector of the atmosphere with respect to the spacecraft. The atmospheric density, $\rho_a(t)$, is calculated using the Marshall Engineering Thermosphere model,[14] which accounts for seasonal and diurnal heating effects of the Earth's atmosphere. The drag coefficient, C_D, is assumed to be constant for a given orientation of the spacecraft. Also, $S(t)$ is the attitude dependent frontal area and $\boldsymbol{\rho}_{cp}(t)$ is the attitude dependent center of pressure location with respect to the center of mass. The relative velocity vector $\mathbf{v}_r(t)$ can be approximated with the assumption that the atmosphere co-rotates with the Earth:[15]

$$\mathbf{v}_r(t) = \mathbf{v}(t) - \boldsymbol{\omega}_\oplus \times \boldsymbol{r}(t) \tag{6}$$

where $\mathbf{v}(t)$ is the inertial spacecraft velocity vector, $\mathbf{r}(t)$ is the inertial position vector, and $\boldsymbol{\omega}_\oplus$ is the Earth's angular velocity vector with magnitude of 0.7292×10^{-4} rad/s.

The attitude dependent aerodynamic parameters are calculated with the method developed in Ref. 16, where the reference area and the center of pressure are calculated for any orientation by defining interpolation functions. The projected area and the center of pressure

for the three orthogonal body reference axes of the ISS are given in Ref. 1 for each assembly stage.

The vent torque is modeled by

$$\boldsymbol{N}_{vent}(t) = \boldsymbol{r}_{vent} \times \boldsymbol{F}_{vent}(t) \tag{7}$$

where $\boldsymbol{r}_{vent}$ is the moment arm of a vent torque from the center of mass to a leak location, which is assumed to be a constant vector, and $\boldsymbol{F}_{vent}(t)$ is a time-varying vent thrust vector. The effects of flexible body dynamics are not considered in this research. Detailed studies on the flexible space station attitude dynamics can be found in Refs. 17–19 and 20.

Vent Thrust Calculation

A leak hole perforated on the surface of a pressurized module will behave like a short length nozzle. The dynamic properties of the air flow through the leak hole are analyzed using one-dimensional isentropic and isothermal nozzle dynamic models. Figure 1 shows a diagram of the air flow through the leak hole on the pressurized module, where T^* and P^* are the temperature and pressure of the air in the leak hole, respectively, T and P are the temperature and pressure of the inside of the pressurized module, respectively, $\boldsymbol{F}_{vent}$ is the vent thrust, and P_B is the back pressure. The mass flow rate in a leak hole is given by[21]

$$\dot{m}_{out}(t) = -\frac{A(t)P^*(t)v^*(t)}{RT^*(t)} \tag{8}$$

where $A(t)$ is the area of the hole, R is the ideal gas constant (287 N-m/Kg-K), and $v^*(t)$ is the exhaust velocity of the air satisfying

$$v^*(t) = \sqrt{\gamma R T^*(t)} \tag{9}$$

where γ is the specific heat ratio, with $\gamma = 1.4$ for an ideal gas. The mass flow rate, $\dot{m}_{out}(t)$, can be expressed as a function of the air inside the pressurized module. This is accomplished

by substituting the following expressions into Eq. (8):

$$P^*(t) = P(t) \left(\frac{2}{\gamma + 1} \right)^{\frac{\gamma}{\gamma - 1}} \tag{10a}$$

$$T^*(t) = T(t) \left(\frac{2}{\gamma + 1} \right) \tag{10b}$$

yielding

$$\dot{m}_{out}(t) = -\frac{A(t)P(t)\sqrt{\gamma}}{\sqrt{RT(t)}} \left(\frac{2}{1 + \gamma} \right)^{\frac{1+\gamma}{2(\gamma-1)}} \tag{11}$$

The actual mass flow rate can be calculated by multiplying $\dot{m}_{out}$ in Eq. (8) by the discharge coefficient C_J. The discharge coefficient is defined by the relation:

$$C_J = \frac{\text{actual velocity at nozzle exit}}{\text{velocity at nozzle exit with isentropic flow}} \tag{12}$$

and depends on the shape of the exit orifice (for a round orifice, $C_J = 0.8$).

Using the thrust equation the vent thrust magnitude is given by

$$||\boldsymbol{F}_{vent}(t)|| = C_J \dot{m}_{out}(t)v^*(t) + [P^*(t) - P_a(t)]A(t) \tag{13}$$

where P_a is the ambient pressure, which is approximately zero for the vacuum of space. Substituting Eqs. (8), (9) and (10) into Eq. (13), and simplifying yields

$$||\boldsymbol{F}_{vent}(t)|| = A(t)P(t) (C_J \gamma + 1) \left(\frac{2}{\gamma + 1} \right)^{\frac{\gamma}{\gamma - 1}} \tag{14}$$

Note that the magnitude of the vent thrust is proportional to the pressure inside the module and to the area of the leak hole. This expression is very useful since the vent thrust magnitude is a direct function of the internal pressure, $P(t)$, which can be measured by a pressure sensor. For the calculation of the hole area, $A(t)$, the following approach is used. The indication of an air leak in a pressurized module is the depressurization of the air. The air inside the

module follows the ideal gas law, given by

$$P(t) = \frac{m(t)RT(t)}{V(t)} \quad \text{or} \quad m(t) = \frac{P(t)V(t)}{RT(t)} \tag{15}$$

where $V(t)$ is the volume of the air and $m(t)$ is the air mass inside the volume. Differentiating the second equation of Eq. (15) with respect to time yields

$$\dot{m}(t) = \dot{m}_{out}(t) + \dot{m}_{in}(t) = \frac{\dot{P}(t)V(t)}{RT(t)} + \frac{P(t)\dot{V}(t)}{RT(t)} - \frac{P(t)V(t)\dot{T}(t)}{RT^2(t)} \tag{16}$$

In this equation, the mass flow rate, $\dot{m}(t)$, can be decomposed into two parts: 1) the air mass introduction rate from a ventilation system, $\dot{m}_{in}(t)$, and 2) the air mass expulsion due to a leak, $\dot{m}_{out}(t)$. Therefore, Eq. (16) can be rewritten, assuming constant volume V, as

$$\dot{m}_{out}(t) = \frac{\dot{P}(t)V}{RT(t)} - \frac{P(t)V\dot{T}(t)}{RT^2(t)} - \dot{m}_{in}(t) \tag{17}$$

If we know the internal pressure $P(t)$ and the temperature $T(t)$ and their respective rate, and $\dot{m}_{in}(t)$, the area of a the leak hole, $A(t)$, can be calculated by equating Eqs. (11) and (17), which yields

$$A(t) = -\frac{\sqrt{RT(t)}}{P(t)\sqrt{\gamma}} \left(\frac{2}{1+\gamma}\right)^{\frac{1+\gamma}{2(1-\gamma)}} \left[\frac{\dot{P}(t)V}{RT(t)} - \frac{P(t)V\dot{T}(t)}{RT^2(t)} - \dot{m}_{in}(t)\right] \tag{18}$$

The thrust can be calculated by substituting Eq. (18) into Eq. (14).

We can further simplify the thrust calculation when there is no mass introduction, $\dot{m}_{in} \simeq 0$, in the volume and by making some assumptions for the depressurization process model. We consider two special process models based on the temperature characteristics of the air. For an isentropic air model, which involves no heat transfer (adiabatic) and no irreversibilities

within the system, $P(t)$ and $T(t)$ are related by

$$T(t) = T_0 \left(\frac{P(t)}{P_0} \right)^{\frac{\gamma-1}{\gamma}} \tag{19}$$

and the depressurization rate $\dot{P}(t)$ can be derived by using Eqs. (17) and (19), giving

$$\dot{P}(t) = -k_1 A(t) P^{k_2}(t) \tag{20a}$$

$$k_1 = \frac{\gamma \sqrt{RT_0\gamma}}{V} P_0^{\frac{1-\gamma}{2\gamma}} \left(\frac{2}{\gamma+1} \right)^{\frac{\gamma+1}{2(\gamma-1)}} C_J \tag{20b}$$

$$k_2 = \frac{3\gamma-1}{2\gamma} \tag{20c}$$

where the subscript 0 stands for the initial value, and k_1 and k_2 are constants.

Another process model we consider is the isothermal process, where the temperature T is treated as a constant in Eq. (17). The depressurization rate, $\dot{P}(t)$, in this case can be derived as

$$\dot{P}(t) = -k_3 A(t) P(t) \tag{21a}$$

$$k_3 = \frac{\sqrt{RT\gamma}}{V} \left(\frac{2}{1+\gamma} \right)^{\frac{1+\gamma}{2(\gamma-1)}} C_J \tag{21b}$$

where k_3 is constant. Note that we cannot use Eq. (19) anymore for the isothermal process and that the actual temperature T of the air appears in the process equation.

Comparisons between the isentropic and isothermal gas model are shown in Figures 2 and 3, using the ISS assembly Stage 16A with a leak hole radius of 0.3 inch and a pressurized volume of 867.2 m^3. From Figure 2, the isentropic gas model gives a faster pressure drop in the internal pressure than the isothermal gas model. Therefore, the reserve time t_{res}, which is a measure of the time it takes for the current pressure $P(t)$ to reach the minimum habitable pressure, $P_{min} \approx 490$ mmHg $= 6.530 \times 10^4$ Pa, is shorter using the isentropic gas model than using the isothermal gas model. The reserve time t_{res} can be obtained by integrating

Eq. (20a) for the isentropic process and Eq. (21a) for the isothermal process. The reserve time for the isentropic process is

$$t_{res} = \frac{\left(\frac{P_{min}}{P(t)}\right)^{\frac{1-\gamma}{2\gamma}} - 1}{\frac{\gamma-1}{2}\frac{A(t)}{V}\sqrt{RT(t)\gamma}\left(\frac{2}{\gamma+1}\right)^{\frac{\gamma+1}{2(\gamma-1)}}C_J} \tag{22}$$

where the internal temperature $T(t)$ can be substituted by $P(t)$ from Eq. (19). From Figure 3 the vent thrust magnitude is larger using the isothermal gas model, meaning the isothermal gas model produces a greater torque than the isentropic gas model. Also, as can be clearly seen, the differential pressure dominates the mass propulsion effect. But note that there isn't much difference in vent thrust magnitude for both gas models just after the vent starts (e.g. within 10 minutes).

Vent Thrust Estimation

Since the actual internal pressure measurements are corrupted by noise, the continuous-discrete Kalman filter[22] is used to estimate the hole area, $A(t)$, which is needed to calculate the magnitude of vent thrust with Eq. (14). The state equations for the depressurization process have the following form:

$$\dot{\boldsymbol{x}}(t) = \boldsymbol{f}\left[\boldsymbol{x}(t), t\right] + \boldsymbol{\eta}(t) \tag{23}$$

where the state $\boldsymbol{x}(t) = [P(t),\ A(t)]^T$ and

$$\boldsymbol{f}\left[\boldsymbol{x}(t), t\right] = \begin{bmatrix} -k_1 A(t) P^{k_2}(t) \\ 0 \end{bmatrix} \tag{24}$$

for an isentropic process model, and

$$\boldsymbol{f}\left[\boldsymbol{x}(t), t\right] = \begin{bmatrix} -k_3 A(t) P(t) \\ 0 \end{bmatrix} \tag{25}$$

for an isothermal process model. The vector $\boldsymbol{\eta}(t) = [\eta_1(t),\ \eta_2(t)]^T$ is the process noise, where $\eta_1(t)$ and $\eta_2(t)$ are Gaussian white-noise processes with

$$E\left\{\eta_i(t)\right\} = 0 \tag{26a}$$

$$E\left\{\eta_i(t)\eta_j(t')\right\} = Q\delta_{i,j}(t-t') \tag{26b}$$

with $i,\ j = 1,\ 2$. The matrix Q has the following form

$$Q = \begin{bmatrix} \sigma_1^2 & 0 \\ 0 & \sigma_2^2 \end{bmatrix} \tag{27}$$

where the terms σ_1^2 and σ_2^2 are the variances of $\eta_1(t)$ and $\eta_2(t)$, respectively. The strength of the noise σ_2 corresponds to the possible range of the area variation. The discrete-time internal pressure measurement, denoted by $\tilde{y}_k$, is modeled as

$$\tilde{y}_k = P_k + v_k \tag{28}$$

where v_k is the measurement noise, which satisfies a discrete Gaussian white-noise process with

$$E\left\{v_k\right\} = 0 \tag{29a}$$

$$E\left\{v_k v_{k'}\right\} = R_k \delta_{k,k'} \tag{29b}$$

The standard continuous-discrete extended Kalman filter algorithm[22] can now be applied to estimate the pressure and area to calculate the magnitude of the vent thrust with Eq. (14). Note that for the initial condition of the filter, the following value is used: $\hat{\boldsymbol{x}}(t_0) = [\tilde{y}_0 \ 0]^T$.

Vent Torque Estimation

The vent torque, which is not explicitly modeled in the attitude dynamics, shows up as a residual disturbance torque when the spacecraft angular rate measurement undergoes a filtering process. In the vent torque estimation algorithm, another filter is executed whose state vector is augmented to include the unknown parameters as additional states, resulting in a total of six filter states, where three states are for the total angular momentum of the spacecraft and the other three states are for the three-axis components of the disturbance torque. Note that the attitude information, which is needed to determine the gravity-gradient and aerodynamic torque in the disturbance torque estimation algorithm, is assumed to be available from a real-time attitude estimation algorithm. In this section, the disturbance estimation algorithm using the UF approach is shown.

The state model for the torque estimation filter with $\boldsymbol{x}(t) = [\boldsymbol{H}(t)^T, \ \boldsymbol{N}_{vent}(t)^T]^T$ can be expressed as

$$
\begin{bmatrix} \dot{\boldsymbol{H}}(t) \\ \dot{\boldsymbol{N}}_{vent}(t) \end{bmatrix} = \begin{bmatrix} -J^{-1}\left[\boldsymbol{H}(t) - \boldsymbol{h}(t)\right] \times \ \boldsymbol{H}(t) + \boldsymbol{L}(t) + ||\boldsymbol{F}_{vent}(t)||\boldsymbol{N}_{vent}(t) \\ \boldsymbol{0}_{3\times 1} \end{bmatrix} + \begin{bmatrix} \boldsymbol{\eta}_H(t) \\ \boldsymbol{\eta}_N(t) \end{bmatrix}
\tag{30}
$$

where $||\boldsymbol{F}_{vent}(t)||\boldsymbol{N}_{vent}(t)$ is the vent disturbance torque. Note that $\boldsymbol{H}(t)$ and J are calculated with respect to the body-fixed frame with its origin at the center of mass. This form of Euler's equation is preferred since it does not involve a derivative of the CMG wheel speed, $\dot{\boldsymbol{h}}(t)$, which may contain significant noise. The thrust magnitude, $||\boldsymbol{F}_{vent}(t)||$, is treated as a deterministic quantity and is estimated from the EKF algorithm shown earlier. The vectors $\boldsymbol{\eta}_H(t)$ and $\boldsymbol{\eta}_N(t)$ are zero-mean Gaussian process noise vectors, which correspond roughly to the possible range of the disturbance variations. The attitude dependent torque, $\boldsymbol{L}(t)$, is

the external disturbance, expressed as

$$\boldsymbol{L}(t) = \boldsymbol{N}_{drag}(t) + \boldsymbol{N}_{grav}(t) \tag{31}$$

neglecting other sources of disturbance. This vector is treated as a deterministic input in the filter equations. The discrete gyroscope output measurement model is

$$
\begin{aligned}
\tilde{\boldsymbol{y}}_k &= \boldsymbol{\omega}_k + \boldsymbol{\eta}_{1_k} \\
&= J^{-1}\left[\boldsymbol{H}_k - \boldsymbol{h}_k\right] + \boldsymbol{\eta}_{1_k}, \quad k = 1, \ldots, N
\end{aligned} \tag{32}
$$

An UF approach is considered here as an alternative to the EKF for this particular estimation problem. The UF has first been proposed by Julier and Uhlman 6. Unlike the EKF, the UF more accurately captures the posterior mean and covariance of a random variable for any nonlinearity by choosing a minimal set of sample points and propagating them through the original nonlinear system. Also it is derivative-free, i.e. no Jacobian and Hessian calculations need to be evaluated for the computation. Therefore, it can be easily applied to any complex dynamical system and to non-differentiable functions. For disturbance estimation, the UF approach has faster convergence compared to the EKF in the presence of large initial errors in the filter states.[23] The continuous-time nonlinear equations shown in Eqs. (30) and (32) can be discretized to fit the UF derivation shown in Ref. 6 through an appropriate numerical integration scheme.

Numerical simulations for the UF cases are performed with an angular rate-noise standard deviation of 2.3×10^{-4} °/sec ($\sigma_1 = 4 \times 10^{-6}$ rad/sec) and a sampling frequency of 1 Hz for the ISS assembly stage UF1. It is assumed that the spacecraft attitude maintains the TEA when suddenly after 5.7556 hr (20720 sec) a vent torque of 66.07 Nm is applied in each body axis of the spacecraft. The disturbance torque estimation results after the onset of venting are shown in Figure 4, where the dashed lines correspond to the true values. We can see that the vent torque estimates converge to the true values around 10 seconds after the

leak. When an air leak occurs, the state covariance of the filter is reset to a large value to incorporate the variation of the disturbance torque at the instant when the leak occurs (as previously mentioned, it is known when a leak occurs by sensing the air pressure drop inside the crew cabin). In this way the filter converges much faster than without a covariance reset. The estimation errors for each component of the disturbance torque, denoted by $\Delta \boldsymbol{N}_{vent}$, are shown in Figure 5 with their 3σ-bound lines.

Inertia Estimation

For the ISS, the uncertainty in the aerodynamic torque may affect the vent torque estimation results if it has the same order of magnitude as the torque due to a leak. But the major uncertainty in the residual torque estimation is the inaccurate ISS inertia mass components. For the ISS, the inertia of each configuration is pre-calculated on the ground with CAD tools. But these values may be imprecise since the ISS is made up of multiple complex rigid bodies interconnected to each other and undergoes several configuration changes during its lifetime. Therefore, an online parameter estimation method is employed to estimate these slowly changing inertia components in real time when it is known that there is no venting leak acting on the spacecraft. But the parameter estimation performance depends heavily on the observability of the parameters of interest. Usually, in the parameter estimation problem, the state vector is extended by adjoining it with the vector of unknown parameters, as has been done for the vent torque estimation algorithm. In this section, a least-squares approach is used to analyze the relative observability of the ISS inertia components.

When the ISS attitude is near the LVLH orientation, the inertia matrix components are unobservable, even though there are some slight attitude variations due to the time varying aerodynamic torque. Assuming that the aerodynamic parameters are known, the inertia matrix observability in an ideal LVLH fixed mode can be shown from the following equations:

$$J_{23} = \frac{1}{4n^2}(N_{aero_1} - u_1)$$

$$J_{13} = \frac{1}{3n^2}(u_2 - N_{aero_2})$$

$$J_{12} = \frac{1}{n^2}(u_3 - N_{aero_3}) \tag{33}$$

where the constant angular rate $\boldsymbol{\omega} = [0 \ -n \ \ 0]^T$ and the constant attitude Euler angles of $[0 \ 0 \ 0]^T$ are substituted in the rotational Euler's equation of motion. The quantities N_{aero_i} and u_i are the ith component of the aerodynamic torque and the control torque input, respectively, and J_{ij} is the ij^{th} inertia matrix element. The spacecraft is assumed to be rotating in an Earth-pointing mode with a constant attitude angular rate $n = 0.0011$ rad/sec. We can see from Eq. (33) that among the six inertia components, only the products of inertia (J_{23}, J_{13} and J_{12}) show up due to the presence of the gravity-gradient torque. But note that the control input, $\boldsymbol{u}$, and the aerodynamic torque, $\boldsymbol{N}_{aero}$, have small values with the same order of magnitude. Therefore, exact knowledge of the aerodynamic and control input torque are needed to directly calculate the products of inertia, which is actually not feasible in practice.

A numerical test is done with the batch least-squares method to check the observability conditions in the LVLH fixed attitude mode. The assumptions are: 1) perfect measurements of the attitude, angular rate, control input and the angular acceleration are available, 2) perfect knowledge of the aerodynamic torque, and 3) no other disturbances besides aerodynamic and gravity-gradient torque are present. A linear parametrization of the equations of motion is needed to use the batch least-squares method. At known discrete instants of time t_j, Euler's equation can be linearly parameterized with respect to the unknown inertia components as

$$
\begin{aligned}
-\boldsymbol{u}(t_j) + \boldsymbol{N}_{aero}(t_j) &= J\dot{\boldsymbol{\omega}}(t_j) + \boldsymbol{\omega}(t_j) \times [J\boldsymbol{\omega}(t_j)] - 3n^2 \boldsymbol{C}_3(t_j) \times [J\boldsymbol{C}_3(t_j)] \\
&= \{D_1[\dot{\boldsymbol{\omega}}(t_j)] + D_2[\boldsymbol{\omega}(t_j)] - 3n^2 D_2[\boldsymbol{C}_3(t_j)]\} \boldsymbol{J} \\
\tilde{\boldsymbol{y}}(t_j) &= \boldsymbol{h}(t_j)\boldsymbol{J}, \quad j = 1, 2, ..., m
\end{aligned} \tag{34}
$$

where $\boldsymbol{J} = [J_{11}\ J_{22}\ J_{33}\ J_{23}\ J_{13}\ J_{12}]^T$, and the matrices D_1 and D_2 are defined as[8]

$$D_1(\dot{\boldsymbol{\omega}}) = \begin{bmatrix} \dot{\omega}_1 & 0 & 0 & 0 & \dot{\omega}_3 & \dot{\omega}_2 \\ 0 & \dot{\omega}_2 & 0 & \dot{\omega}_3 & 0 & \dot{\omega}_1 \\ 0 & 0 & \dot{\omega}_3 & \dot{\omega}_2 & \dot{\omega}_1 & 0 \end{bmatrix} \tag{35}$$

$$D_2(\boldsymbol{\omega}) = \begin{bmatrix} 0 & -\omega_2\omega_3 & \omega_2\omega_3 & \omega_2^2 - \omega_3^2 & \omega_1\omega_2 & -\omega_1\omega_3 \\ \omega_1\omega_3 & 0 & -\omega_1\omega_3 & -\omega_1\omega_2 & \omega_3^2 - \omega_1^2 & \omega_2\omega_3 \\ -\omega_1\omega_2 & \omega_1\omega_2 & 0 & \omega_1\omega_3 & -\omega_2\omega_3 & \omega_1^2 - \omega_2^2 \end{bmatrix} \tag{36}$$

and m is the number of measurements. The solution of the least-squares method for the estimation of the inertia matrix is as follows:

$$\boldsymbol{J} = (H^T H)^{-1} H^T \tilde{\boldsymbol{Y}} \tag{37}$$

where the quantities H and $\tilde{\boldsymbol{Y}}$ are known from the measurements and the control inputs:

$$\tilde{\boldsymbol{Y}} = [\tilde{\boldsymbol{y}}(t_1)^T,\ \tilde{\boldsymbol{y}}(t_2)^T,\ ...,\ \tilde{\boldsymbol{y}}(t_m)^T]^T \tag{38}$$

$$H = [\boldsymbol{h}(t_1)^T,\ \boldsymbol{h}(t_2)^T,\ ...,\ \boldsymbol{h}(t_m)^T]^T \tag{39}$$

The quantity $H^T H$ should be strictly positive definite since its inverse appears in Eq. (37) to solve the unknown parameters. In practice, we require $H^T H$ to be well-conditioned. A useful measure of the condition of a matrix is the condition number.[24] The condition number varies from 1 for an orthogonal matrix to infinity for a singular matrix. From a numerical simulation, when all six components of inertia matrix are solved using the Eq. (37), the condition number of $H^T H$ is 1.7×10^{10}, resulting in an inaccurate solution. The relative observability among the inertia components is analyzed using an eigenvalue/eigenvector decomposition of the $H^T H$ matrix, which is shown in Figure 6. From this figure, J_{11} is the maximum component of the eigenvector, which corresponds to an eigenvalue of magnitude

10^{-15}. As expected the three products of inertia, which have their eigenvalues near 10^{-6} are the most observable components among the elements, whereas the three moments of inertia have their magnitude near 10^{-15}, which is nine orders of magnitude smaller than those of the products of inertia. A simulation has been done to estimate the products of inertia with a batch least-squares method, and the results are shown in Figure 7 (where the results are calculated at regular instants of time with the cumulative measurements). The three components converge very quickly, within an orbit, to their true values (expressed as circles in the figure) as expected. The corresponding condition number is 16, which is much smaller than the previous simulation case, revealing that the $H^T H$ is now a well-conditioned matrix. For the real-time estimation of the inertia, the UF approach is used because of its robustness in the presence of large initial state uncertainty and its derivative free characteristics. The UF filter formulation is similar to the vent torque estimation approach with the filter state $\boldsymbol{x}(t) = [\boldsymbol{H}(t)^T \; J_{11} \; J_{22} \; J_{33} \; J_{23} \; J_{13} \; J_{12}]^T$ using the dynamic equation shown in Eq. (1).

The center of mass is also estimated, since this quantity is also needed in the leak localization algorithm. For the center of mass estimation, we can rewrite the rotational equation of motion of the ISS about the center of mass as

$$J\dot{\boldsymbol{\omega}}(t) + \boldsymbol{\omega}(t) \times [J\boldsymbol{\omega}(t)] = \boldsymbol{L}(t) + \boldsymbol{N}_{CMG}(t) + \sum_{i=1}^{n} \boldsymbol{r}_i \times \boldsymbol{F}_i(t) \tag{40}$$

where $\boldsymbol{F}_i(t)$ is the ith applied force vector and $\boldsymbol{r}_i$ is the moment arm from the center of mass. The coordinate of the moment arm can be expressed as

$$\boldsymbol{r}_i = \boldsymbol{l}_i - \boldsymbol{d} \tag{41}$$

where $\boldsymbol{l}_i$ is the known position vector of the point of the applied force, $\boldsymbol{F}_i(t)$, and $\boldsymbol{d}$ is the unknown position vector of the center of mass, both expressed with respect to the body-fixed frame with a known origin. The torque due to the CMGs, $\boldsymbol{N}_{CMG}(t)$, does not depend on each CMG location, but is a function of the orientation of each CMG. Therefore to

estimate the center of mass position, a control torque (thruster) with known position and magnitude needs to be applied to the spacecraft. Then the filter state must be augmented to include three elements of $\boldsymbol{d}$ for the estimation of the center of mass (estimation of the six inertia elements may be estimated concurrently). Estimation of the mass properties should be performed only when an attitude maneuver is present to enhance the observability of the parameters. Recently, an algorithm to estimate the moments and products of the inertia matrix using a batch process has been developed by Psiaki.[25] This approach uses a trapezoidally integrated version of Euler's equation in inertial coordinates for the filter propagation and incorporates a scalar quadratic constraint to overcome the unobservability of the parameters' overall scaling.

Leak Localization

Once the vent torque, $\boldsymbol{N}_{vent}(t)$, is estimated by the real-time filter, the next step involves determining the position vector $\boldsymbol{r}_{vent}$, which is the moment arm of the vent torque satisfying

$$\boldsymbol{N}_{vent}(t) = \boldsymbol{r}_{vent} \times \boldsymbol{F}_{vent}(t) \tag{42}$$

In the above equation, the vent torque and the magnitude of $\boldsymbol{F}_{vent}(t)$ are known by the estimation algorithms.

The overall steps for locating a leak on the ISS are as follows:

1. Model the 3-D geometric surfaces of the pressurized parts of the spacecraft.

2. Estimate the vent torque and magnitude of the vent thrust.

3. Slice the 3-D surfaces of the pressurized modules with a plane perpendicular to the direction of the vent torque so that this plane includes the center of mass of the spacecraft. From the fundamental definition of torque, a torque about the center of mass of a rigid body is perpendicular to the plane comprising the vectors $\boldsymbol{r}_{vent}$ and $\boldsymbol{F}_{vent}$. So, $\boldsymbol{r}_{vent}$, $\boldsymbol{F}_{vent}$ and the center of mass are all in the same plane normal to the

direction of the vent torque. Denote this plane by τ. The intersection between the plane τ and the surface of the spacecraft produces contours.

4. With the assumption that the vent thrust is normal to the tangent plane of the partial section on the ISS surface where the leak occurs, calculate the gradient vectors (direction normal vectors) of the points that make up the sliced contours obtained in Step 3.

5. Multiply the magnitude of the vent thrust estimated in Step 1 with all gradient vectors calculated in Step 4.

6. Since the position and gradient vectors of all the points making the sliced contours are known, calculate the resulting torque at each point on the contours.

7. From the torques obtained for each point in Step 6, select the torques that are closest to the estimated torque (within an error bound) and check their points on the contours.

The actual geometric structure of the station eliminates many of the possible solutions; however, multiple solutions may still exist. In this case further assumptions can be made, such as the probability of impacts by the debris or small meteorites is low on the aft and nadir facing surfaces since these surfaces are shaded by other structures. Also, the leak localization method based on the attitude response may be combined with the conventional leak localization methods. For example, if the solution shows that two possible leaks are situated at two different modules, then only one hatch closure between any of these modules may be needed to check which one of the two modules leaks. Furthermore, visual inspections by the crew may narrow the possible leak solutions.

Numerical Simulation

A user-friendly design tool coded entirely in MATLAB has been developed to estimate a leak location under various conditions. The tool supports several ISS assembly stages from 11A to UF-7, but it may need to be modified due to the uncertainties in the future of the

ISS program. The 3-D surface models of the pressurized segment of the ISS Stage have been developed based on the data provided in Ref. 1. Figure 8 shows the main Graphical User Interfaces (GUIs) of the tool. Users can input the orbit, the mass and the aerodynamic parameters of the ISS, and choose a simulated leak location with the GUI. The resulting leak locations after the leak localization estimation process are shown on another GUI.

For the simulation, the ISS assembly Stage 16A is considered (see Figure 9). The isentropic depressurization process of the air inside the ISS is assumed. The mass and aerodynamic properties of the ISS are provided in Ref. 1. The inertia J is given by

$$J = \begin{bmatrix} 127908568 & 3141229 & 7709108 \\ 3141229 & 107362480 & 1345279 \\ 7709108 & 1345279 & 200432320 \end{bmatrix} (\text{kg m})^2 \tag{43}$$

The centers of pressure are $\boldsymbol{\rho}_{cp_x} = [0, -0.355, -0.927]^T$ m, $\boldsymbol{\rho}_{cp_y} = [-7.94,\ 0, -1.1]^T$ m and $\boldsymbol{\rho}_{cp_z} = [1.12,\ 0.247,\ 0]^T$ m in the Space Station Analysis Coordinate System with respect to the center of mass. The components x, y and z represent the three orthogonal axes of the ISS body fixed frame.[1] The reference projected areas are $S_x = 967$ m^2, $S_y = 799$ m^2 and $S_z = 3525$ m^2.

The Global Positioning System (GPS) attitude-sensor measurement-error standard deviation is given by $\sigma_q = 0.5$ deg, and the ring-laser gyro sensor measurement-error standard deviation is given by $\sigma_\omega = 4 \times 10^{-6}$ deg/sec.[26] The measurement-error standard deviation of the internal pressure is given by $\sigma = 0.1$ mmHg $= 13.3$ Pa. For the depressurization of the air inside, the initial internal temperature and pressure are set to $T_0 = 21^o$ C and $P_0 = 1$ atm, respectively. The back pressure is assumed to be $P_B = 0$ atm and the volume of the entire pressurized system for ISS 16A is $V = 867.2$ m^3. Finally, an inertia uncertainty of 3% is added to the true J.

Simulations are done for 100 seconds from the start of the leak. Figure 10 shows the estimate of the leak hole area using the Kalman filter algorithm. The true leak hole area

A is 1.8241×10^{-4} m^2. As seen from this figure the Kalman filter accurately estimates the leak hole area. The vent thrust magnitude is then computed with the internal pressure measurement and the estimate of the hole area.

For the first simulation, a leak is assumed on a module shown in Figure 11. The sliced plane τ with contours in 3-D is shown in Figure 12. Using the leak localization approach a single leak has been determined for this simulated case, depicted in Figure 13. The estimated position is marked with a $\circ$, the true position of a leak is marked with a $*$ for comparison, and the center of mass is marked with a $\star$ on the plane τ. Slicing of the 3-D surface is performed at the end of the simulation ($t = 100$ sec). If no errors are present in the assumed model and if the assumptions made so far are perfectly satisfied, then the closest torque yielding the point to the estimated vent torque is the true leak point. But because of sensor inaccuracies and modeling errors in the inertia, the estimated vent torque may deviate from the true value. Therefore, an upper error-bound should be set when selecting points that yield the torque closest to the estimated vent torque. For the case shown in Figure 13, we conclude that the leak occurs on the contour line labelled 6, which corresponds to the Kibo JEM pressurized module. In this simulated case, the leak location is well estimated using the new localization method.

Another simulation has been done where multiple locations may result from the given estimated vent torque. In this case, the estimated leak locations are spread over several modules, as shown in Figure 14. The locations P_1, P_2 and P_3 are possible leak candidates (the true leak point is situated near P_1). But since P_1 and P_2 are on the same module, a crew person only needs to close one hatch between the module labelled 20 and the module labelled 19 to verify which one of the two modules has a leak. This is accomplished by measuring the internal pressure drop rate or using visual inspections of the estimated leak points. If the leak hole is due to space debris or small meteorite punctures, then the aft and nadir facing surfaces of the ISS have little possibility to be impacted. This is also true for locations where regions are protected by other structures, as is the case for point P_3.

Therefore this point is not a likely candidate for the leak.

Experimental validation of the algorithm has been treated in Ref. 27, where the effects of the air vent on the attitude of the ISS assembly Stage 5A with the mated Space Shuttle (STS-98) are investigated. The goal involves estimating the torque and the upper bound magnitude of the force caused by the air vent from the depressurization of the Space Shuttle airlock for the preparation of extravehicular activity of the crew. Because a T-shaped valve is used, where air is vented on opposite sides of the valve structure, the net thrust should be nullified in theory. But if the expelled air is not uniform at both openings, a net thrust may occur. From the experimental data it is seen that a CMG momentum buildup occurs during the pressurization process, which means that the net thrust is not cancelled. Actual test data from a depressurization of the space shuttle airlock indicates that the proposed method has the potential to accurately estimate the leak hole size and venting force magnitude (see Ref. 27 for more details).

Conclusions

In this paper, a leak localization method using attitude response data was developed for the International Space Station. The leaking air through the perforated hole on the external surface area leads to a reaction force which results in a torque affecting the attitude of the spacecraft. The size of the leak was calculated from a Kalman filter using estimated values of the internal air pressure and area of the leak hole. The resultant leak torque was estimated by an Unscented filter algorithm. An observability analysis on estimating the inertia components has also been shown. Numerical results showed that the proposed leak localization method can determine a unique solution or multiple solutions. The actual geometric structure of the station eliminates many of the possible solutions; however, multiple solutions may still exist. In this case, further assumptions should be made, such as the probability of impacts by the debris or small meteorites is low on the aft and nadir facing surfaces, and some parts of the surfaces which are not likely to leak can be ignored. Also, the leak localization method based on the attitude response may be combined with the conventional

leak localization methods. For example, if the solution shows that two leaks are situated at two different modules, then only one hatch closure between any of these modules is needed to check which one of the two modules leaks.

Acknowledgements

References

[1]*International Space Station On-Orbit Assembly, Modeling, and Mass Properties Databook: Design Analysis Cycle Assembly Sequence, Revision J*, Lockheed Martin, Houston, TX, 1999, JSC-26557.

[2]*Protecting the Space Station from Meteoroids and Orbital Debris*, National Research Council, Washington, DC, 1997.

[3]Guay, T. D. and Williamsen, J., "International Space Station-Quantifying and Reducing Risk Following Orbital Debris Penetration," *AIAA Space Programs and Technologies Conference*, Huntsville, AL, Sept. 1996, AIAA-1996-4240.

[4]*NASA Space Vehicle Design Criteria, Compartment Venting*, NASA, Washington, DC, Nov. 1970, NASA/SP-8060.

[5]Scialdone, J. J., "Spacecraft Compartment Venting," *Proceedings of SPIE: Optical Systems Contamination and Degradation*, Vol. 3427, Oct. 1998, pp. 23–27.

[6]Julier, S. J., Uhlmann, J. K., and Durrant-Whyte, H. F., "A New Approach for Filtering Nonlinear Systems," *Proceedings of American Control Conference*, Seattle, WA, June 1995, pp. 1628–1632.

[7]Bishop, R. H., Paynter, S. J., and Sunkel, J. W., "Adaptive Control of Space Station with Control Moment Gyros," *IEEE Computer Systems Magazine*, Vol. 12, No. 5, Oct. 1992, pp. 23–28.

[8]Carter, M. T., *Real-Time Analysis of Mass Properties*, Dissertation, Texas A&M University, College Station, Feb. 1999.

[9]Paynter, S. J., *Adaptive Control of the Space Station*, Thesis, University of Texas, Austin, Dec. 1992.

[10]Rochelle, W. C., Reid, E. A., Carl, T. L., and Smith, R. N., "Thermal Analysis for Orbiter and ISS Plume Impingement on International Space Station," *35th AIAA Thermophysics Conference*, Anaheim, CA, June 2001, AIAA-01-31373.

[11]*NASA Space Vehicle Design Criteria, Spacecraft Mass Expulsion Torques*, Dec. 1969.

[12]Sedlund, C. and Sentman, L., "A CAD Method for the Determination of Free Molecule Aerodynamics and Solar Radiation Forces and Moments," *27th Aerospace Sciences Meeting*, Reno, Nevada, Jan. 1989, AIAA-89-0455.

[13]J.R. Wertz, editor, *Spacecraft Attitude Determination and Control*, D. Reidel Publishing Co., Dordrecht, The Netherlands, 1978, p. 567.

[14]Smith, R. E., *The Marshall Engineering Thermosphere (MET) Model Volume I: Technical Description*, NASA, 1998, CR-207946.

[15]Montenbruck, O. and Gill, E., *Satellite Orbits*, chap. 3, Springer, Berlin, Germany, 2001, pp. 83–86.

[16]Carter, M. T., Vadali, S. R., and Chamitoff, G. E., "Parameter Identification for the International Space Station Using Nonlinear Momentum Management Control," *AIAA Guidance, Navigation, and Control Conference*, New Orleans, LA, Aug. 1997, AIAA-1997-3524.

[17]Chang, D. S. and Lee, J. F. L., "Flexible Space Station Attitude Control System Analysis and Design," *AIAA Guidance, Navigation and Control Conference*, Hilton Head Island, SC, Aug. 1992, AIAA-1992-4486.

[18]Sutter, T. R., Cooper, P. A., Young, J. W., and McCutchen, D. K., "Dynamic and Attitude Control Characteristics of an International Space Station," *28th Structures, Structural Dynamics and Materials Conference*, Monterey, CA, April 1987, AIAA-1987-931.

[19]Ashley, H., "Observations on the Dynamic Behavior of Large Flexible Bodies in Orbit," *AIAA Journal*, Vol. 5, March 1967, pp. 460–469.

[20]Segun, T. and Stubbs, N., "Dynamic Analysis of the Space Station Truss Structure Based on a Continuum Representation," *AIAA, ASME, ASCE, AHS, and ASC Structures, Structural Dynamics and Materials Conference*, Mobile, AL, April 1989, AIAA-1989-1280.

[21]Sonntag, R. E., Borgnakke, C., and Wylen, G. J. V., *Fundamentals of Thermodynamics*, chap. 16, John Wiley & Sons, Inc., New York, NY, 5th ed., 1998, pp. 619–630.

[22]Crassidis, J. L. and Junkins, J. L., *Optimal Estimation of Dynamical Systems*, chap. 5, CRC Press, Boca Raton, FL, 2004, pp. 285–292.

[23]Kim, J. W., *International Space Station Leak Localization Using Attitude Response*, Dissertation, Texas A&M University, College Station, Aug. 2002.

[24]Golub, G. H. and Van Loan, C. F., *Matrix Computations*, The Johns Hopkins University Press, Baltimore, MD, 3rd ed., 1996, pp. 80–82.

[25]Psiaki, M. L., "Estimation of a Spacecraft's Attitude Dynamics Parameters by Using Flight Data," *Journal of Guidance, Control, and Dynamics*, Vol. 28, No. 4, July-Aug. 2005, pp. 594–603.

[26]*United States Control Module Guidance, Navigation, and Control Subsystem Design Concept*, NASA, Huntsville, AL, March 1997, MSFC-3677.

[27]Kim, J.-W., Crassidis, J. L., Vadali, S. R., and Dershowitz, A. L., "ISS Leak Localization Using Attitude Response," *AIAA Guidance, Navigation and Control Conference*, Montreal, Canada, Aug. 2001, AIAA-2001-4272.

List of Figures

Figure 1:   Air Flow Through Leak Hole
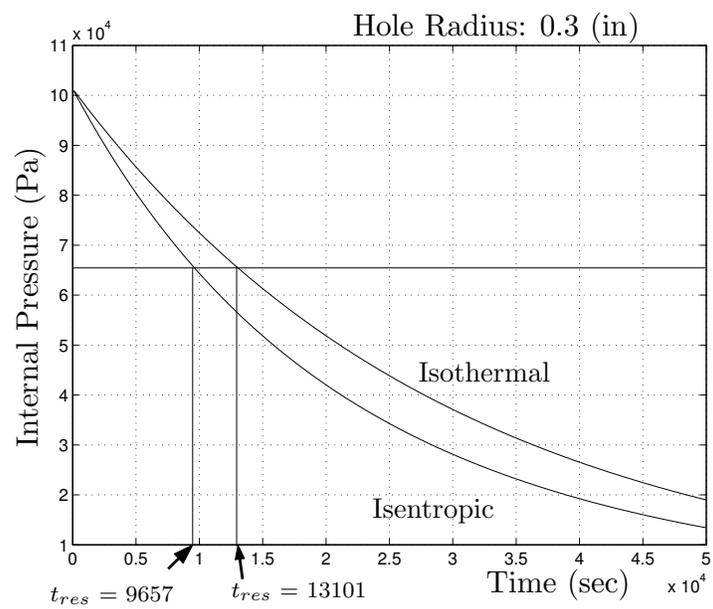
Figure 2:   Internal Pressure

Hole Radius: 0.3 (in)

PSfrag replacements

Vent Thrust (N)

Isothermal

Isentropic

Time (sec)

x 10⁴
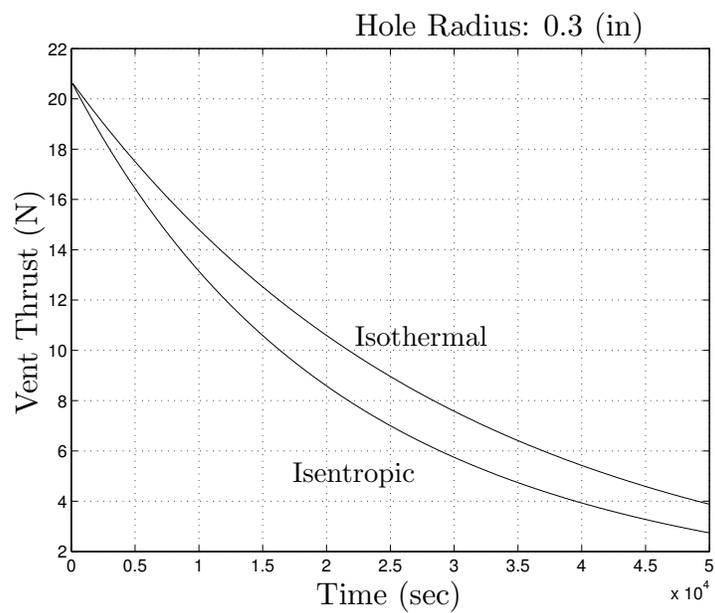
Figure 3:   Vent Thrust Magnitude
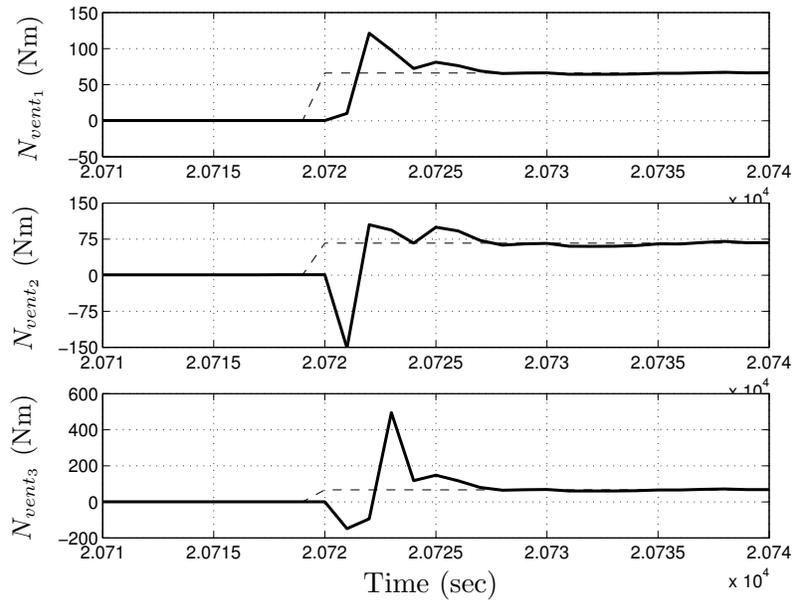
Figure 4: **Vent Torque Estimate Using UF with True Value**
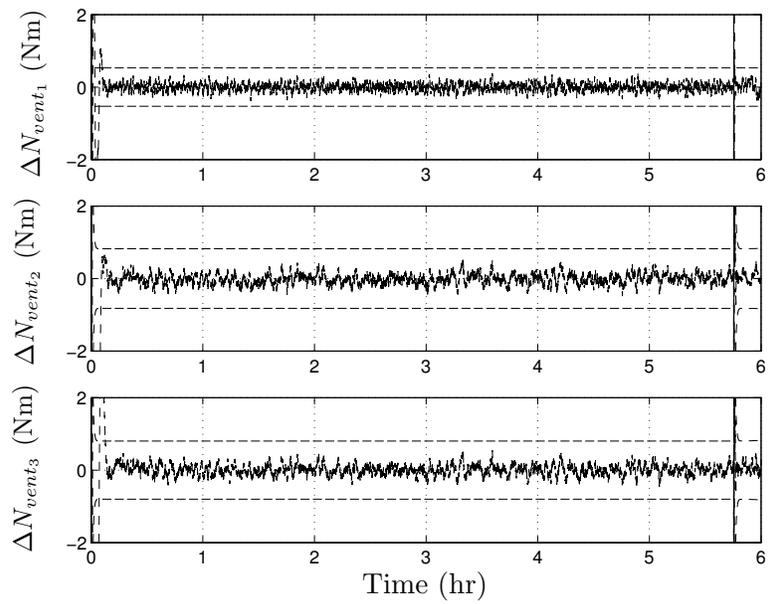
Figure 5: **Disturbance Torque Estimation Error Using UF**
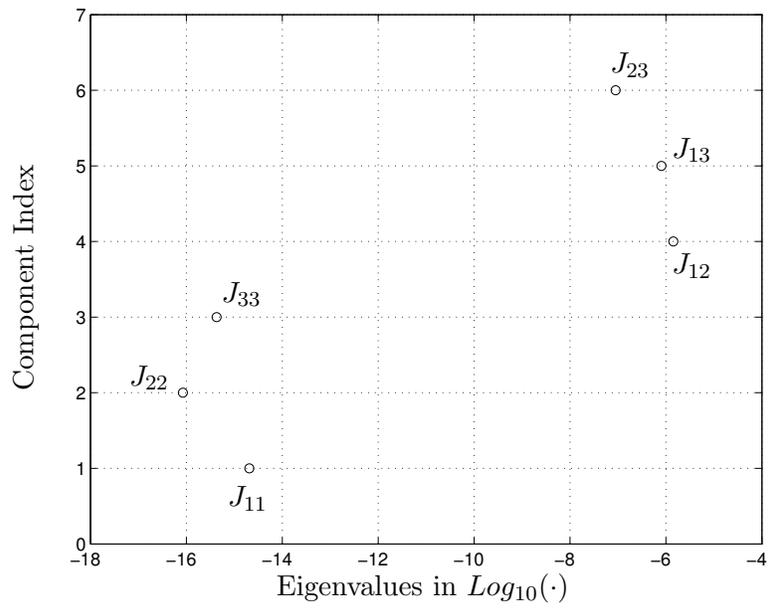
Figure 6: **Relative Observability of Inertia**
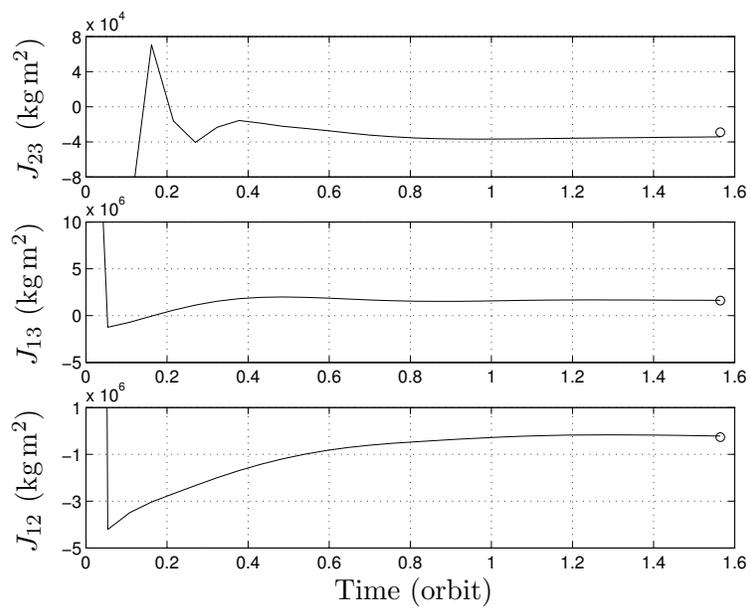
Figure 7: **Inertia Product Estimates Using Least-Squares Method**
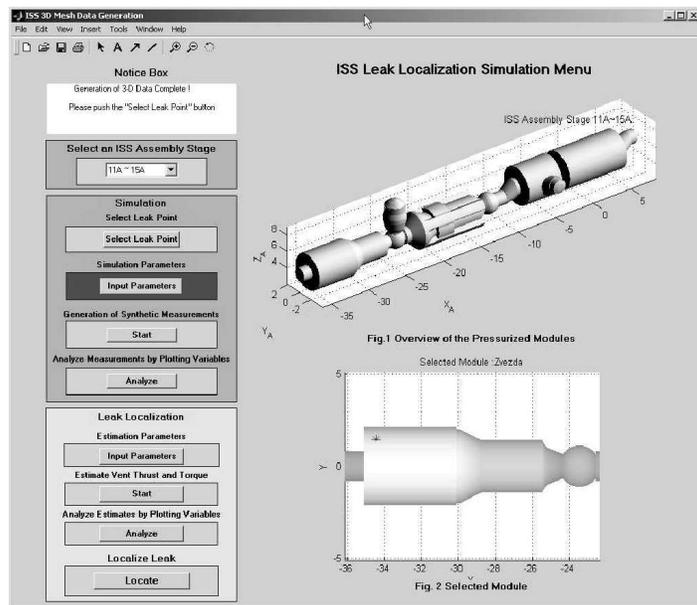
Figure 8:   GUI for Simulation of the Leak Localization Algorithm
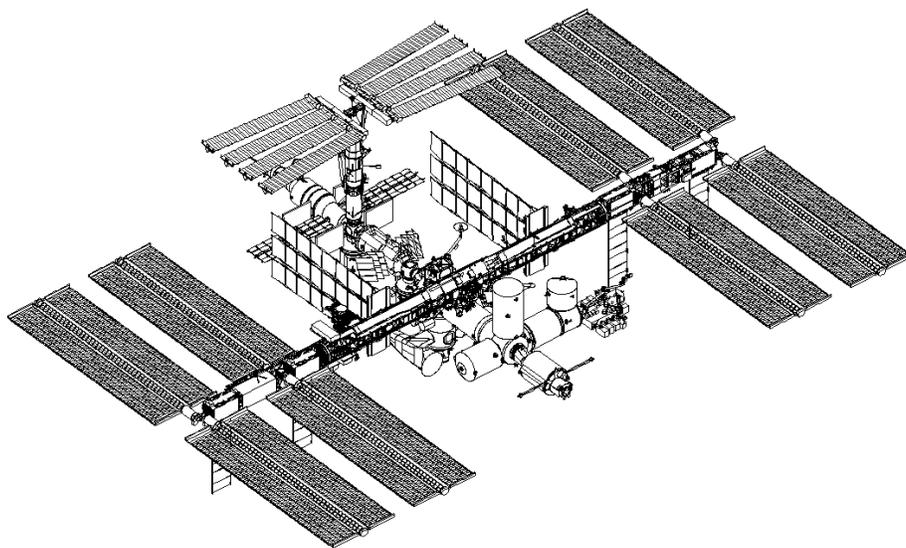
Figure 9:   ISS Assembly Stage 16A
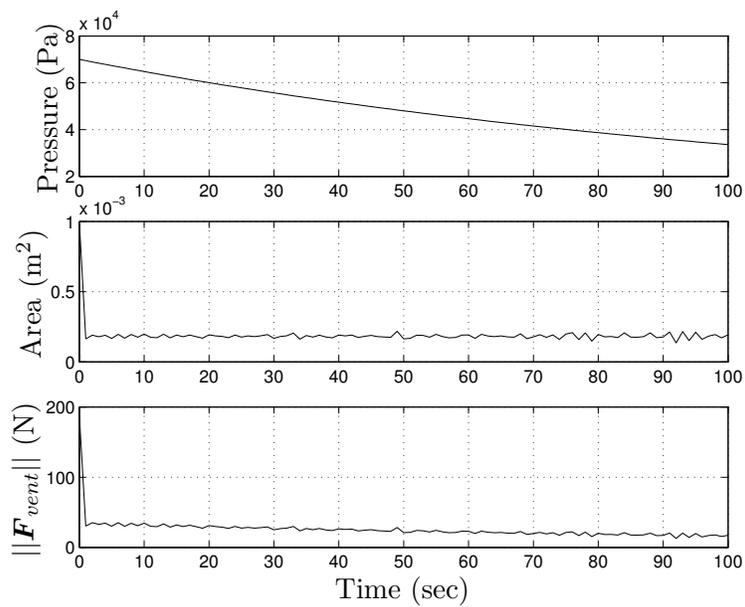
Figure 10: Vent Thrust Magnitude and Hole Area Estimate
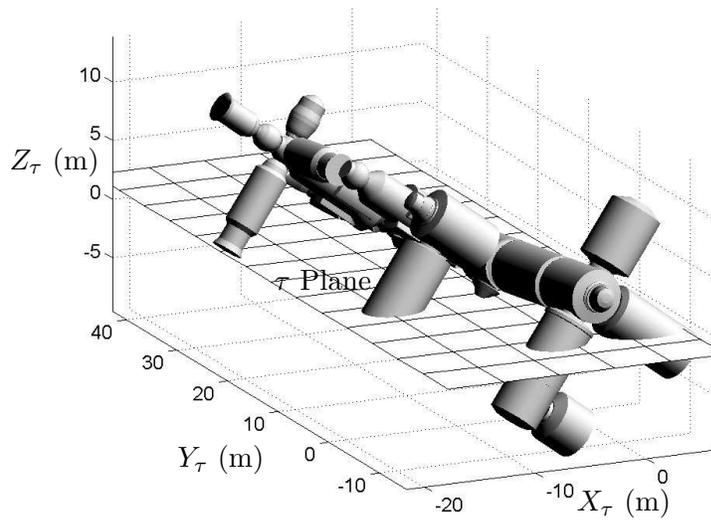
Figure 11:   Slicing 3-D Surface Model with Plane τ

PSfrag replacements
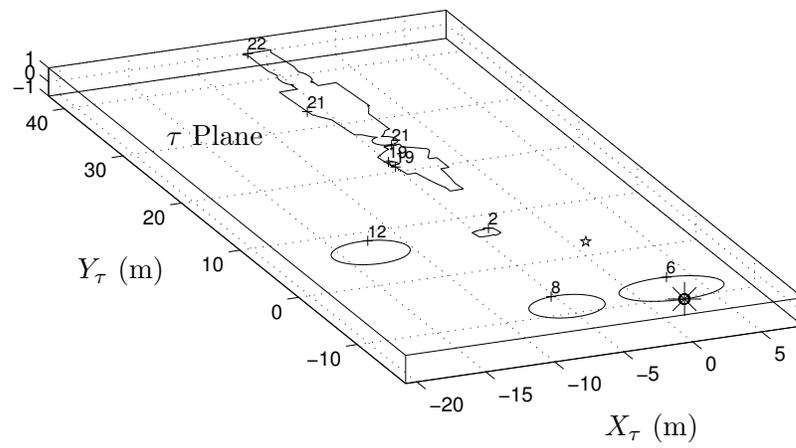
Figure 12: **Sliced Plane τ with Contours in 3-D**

PSfrag replacements
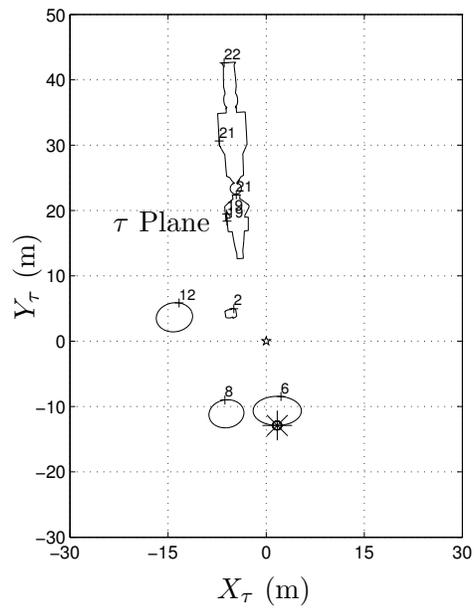
Figure 13: **Contours on Plane τ with Possible Leak**
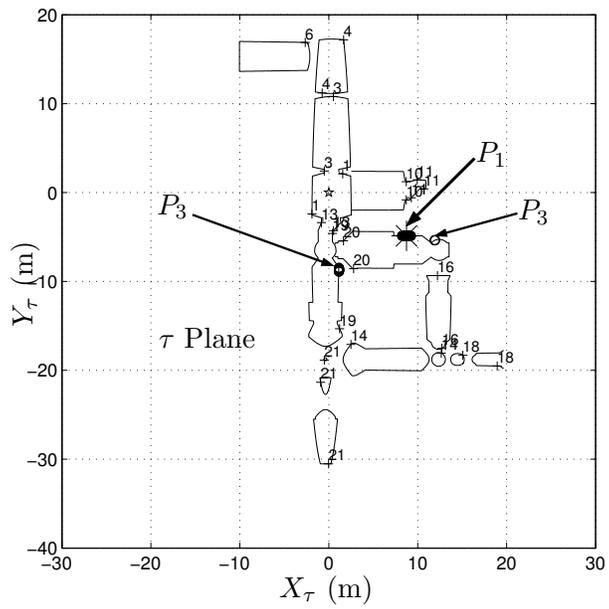
Figure 14: Contours on Plane τ with 3 Possible Leaks